Cell Reports

Report

Transient N-6-Methyladenosine Transcriptome Sequencing Reveals a Regulatory Role of m6A in Splicing Efficiency

Graphical Abstract

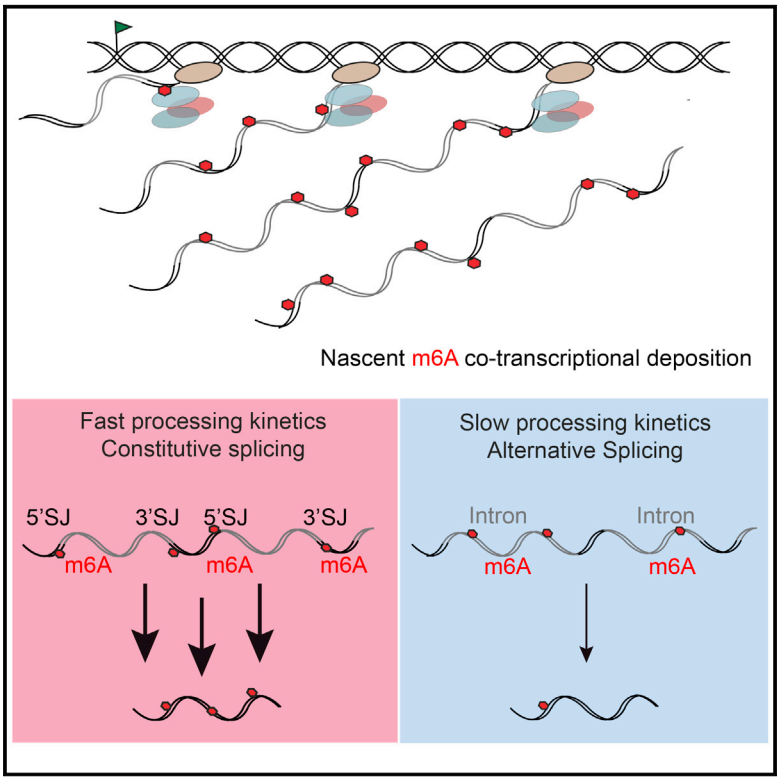

Authors

Annita Louloupi, Evgenia Ntini, Thomas Conrad, Ulf Andersson Vang Ørom

Correspondence

ulf.orom@mbg.au.dk

In Brief

Louloupi et al. describe an approach to detect m6A RNA methylation on nascent RNA. They find that nascent transcripts are often marked by m6A at splice junctions and in introns. The authors show that m6A at splice junctions contributes to faster splicing, while m6A in introns is associated with alternative splicing.

Highlights

- A time-resolved high-resolution picture of m6A on nascent RNA transcripts
- m6A is deposited at nascent RNA and in introns
- m6A deposition at splice-junctions increases splicing kinetics
- High m6A levels in introns is associated with slow and alternative splicing

Data and Software Availability

GSE92565
GSE83561

Louloupi et al., 2018, Cell Reports *23*, 3429–3437
June 19, 2018
https://doi.org/10.1016/j.celrep.2018.05.077

CellPress

Cell Reports
Report

Transient N-6-Methyladenosine Transcriptome Sequencing Reveals a Regulatory Role of m6A in Splicing Efficiency

Annita Louloupi,[1,2,5] Evgenia Ntini,[1,5] Thomas Conrad,[1,3] and Ulf Andersson Vang Ørom[1,4,6,*]
[1]Otto Warburg Laboratories, Max Planck Institute for Molecular Genetics, 14195 Berlin, Germany
[2]Free University, Department of Biology, 14195 Berlin, Germany
[3]BIMSB Genomics, Max Delbrück Center, 13092 Berlin, Germany
[4]Institute for Molecular Biology and Genetics, Aarhus University, 8000 Aarhus, Denmark
[5]These authors contributed equally
[6]Lead Contact
*Correspondence: ulf.orom@mbg.au.dk
https://doi.org/10.1016/j.celrep.2018.05.077

SUMMARY

Splicing efficiency varies among transcripts, and tight control of splicing kinetics is crucial for coordinated gene expression. N-6-methyladenosine (m6A) is the most abundant RNA modification and is involved in regulation of RNA biogenesis and function. The impact of m6A on regulation of RNA splicing kinetics is unknown. Here, we provide a time-resolved high-resolution assessment of m6A on nascent RNA transcripts and unveil its importance for the control of RNA splicing kinetics. We find that early co-transcriptional m6A deposition near splice junctions promotes fast splicing, while m6A modifications in introns are associated with long, slowly processed introns and alternative splicing events. In conclusion, we show that early m6A deposition specifies the fate of transcripts regarding splicing kinetics and alternative splicing.

INTRODUCTION

The RNA nucleotide code is supplemented by more than a hundred chemical modifications, greatly extending the functionality and information content of RNA (Fu et al., 2014; Harcourt et al., 2017). N-6-methyladenosine (m6A) is deposited by a protein complex consisting of the methyltransferase-like 3 and 14 (METTL3 and METTL14), Wilms' tumor 1-associating protein (WTAP), and the Virilizer homolog (KIAA1429) (Liu et al., 2014; Ping et al., 2014; Schwartz et al., 2014). Early studies have demonstrated that adenosine methylation frequently occurs within a subset of RRA*CH consensus sites (R, purine; A*, methylatable A; H, non-guanine base) (Narayan and Rottman, 1988). Fat mass and obesity associated (FTO) and AlkB homolog 5 (ALKBH5) are m6A demethylases, adding dynamics to the function of m6A in RNA biogenesis (Jia et al., 2011; Zheng et al., 2013). m6A is involved in a number of RNA processes, including splicing, RNA degradation, and translation (Bartosovic et al., 2017; Dominissini et al., 2012; Ke et al., 2017; Meyer et al., 2015; Slobodin et al., 2017; Wang et al., 2014; Xiao et al., 2016). These pathways are mediated in part by members of the YTH-domain protein family called m6A readers, which recognize and bind specifically to sequences marked with m6A (Xiao et al., 2016; Xu et al., 2014). The presence of m6A can affect the RNA structure and increase the accessibility of the adjacent RNA sequence for the heterogeneous nuclear ribonucleoproteins HNRNPG and HNRNPC, with an effect on splicing (Liu et al., 2015, 2017). Because of the challenging nature of addressing the impact of m6A on splicing at the mature RNA level, the direct role of m6A on splicing dynamics has not been investigated so far. Here, using TNT-seq (transient N-6-methyladenosine transcriptome sequencing) and qTNTchase-seq (quantitative TNT pulse-chase sequencing), we show that m6A modifications deposited early and co-transcriptionally near splice junctions (SJs) positively affect RNA splicing kinetics. Furthermore, we show that intronic m6A deposition is connected with slow processing kinetics and alternative splicing events. Our results strongly support a scenario where nascent m6A deposition is functionally involved in regulating splicing efficiency (SE) and alternative splicing.

RESULTS

TNT-Seq Reveals m6A Deposition on Newly Transcribed RNA

We developed TNT-seq to identify and study m6A on nascent RNA. In brief, bromouridine (BrU)-labeled RNA was isolated, fragmented, and purified with a BrU-specific antibody. Subsequently, m6A methylated fragments were isolated using an m6A-specific antibody. The labeled RNA (BrU-RNA input) and the m6A-enriched RNA fragments (BrU-m6A-RNA IP eluate) were sequenced to identify positions of m6A on nascent RNA (Figure S1A). We find enrichment of m6A around start and stop codons as well as at 5′ and 3′ SJs reproducibly across independent replicates (Figure S1B), demonstrating a robust experimental pipeline (genome-wide m6A signal correlation = 0.58). The majority (57%) of early m6A peaks (Experimental Procedures) reside within introns, whereas 22% reside in coding sequences (CDSs), 5% are in 5′ UTRs, and 9% are in 3′ UTRs (Figure S1C). To compare m6A peak distribution in newly transcribed RNA with steady-state mRNA, we reanalyzed published m6A-sequencing (m6A-seq)

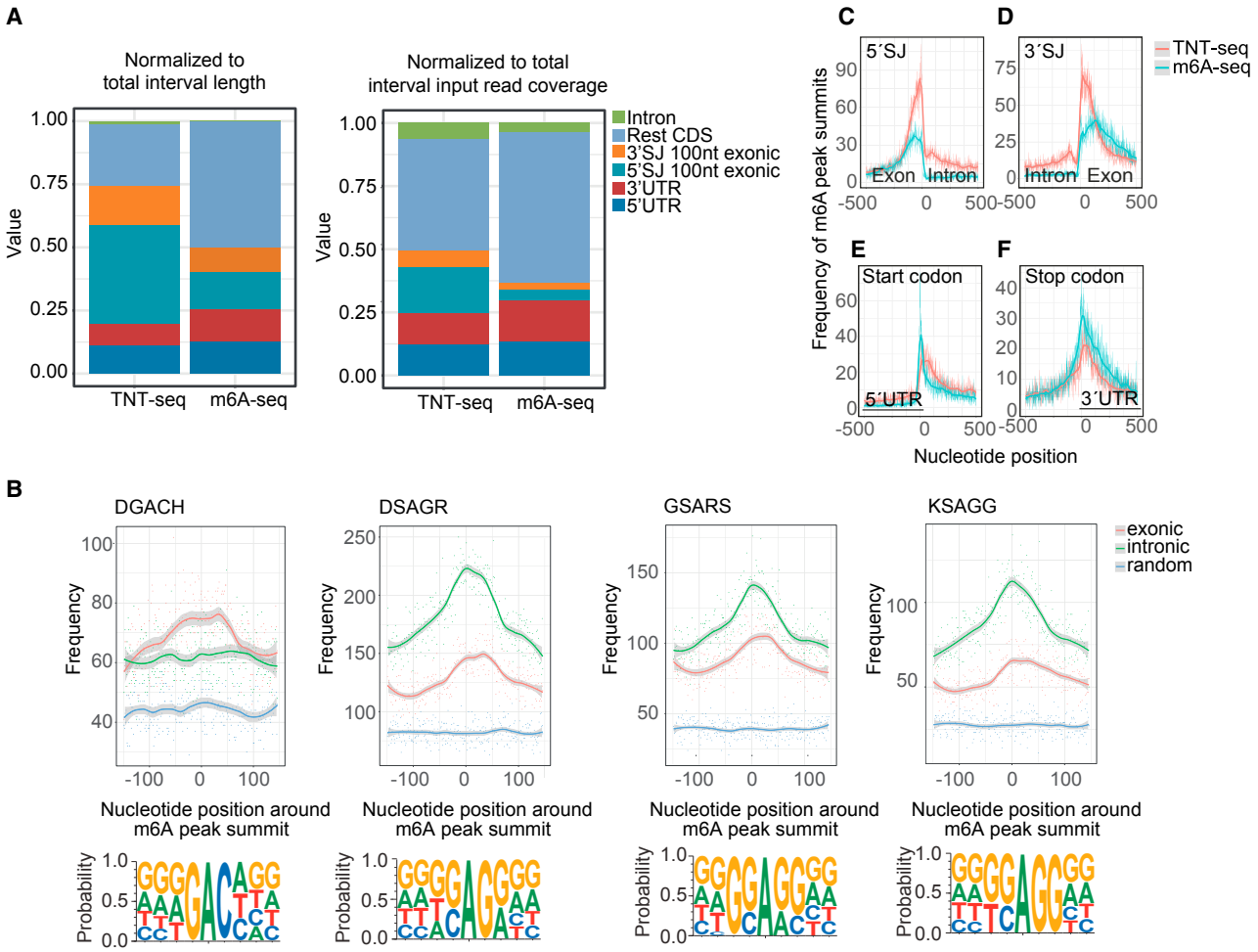

Figure 1. TNT-Seq Reveals m6A Deposition on Newly Transcribed RNA

(A) Distribution of the normalized number of m6A peaks to the length of the analyzed intervals and the respective input read coverage for TNT-seq and mRNA m6A-seq data.

(B) Number of motif occurrences (sum) at nucleotide positions around the m6A peak summit of the top scoring 5,651 exonic peaks, intronic peaks, or random intervals. The line represents loess curve fitting (local polynomial regression), with the 95% confidence interval shaded gray.

(C–F) Distribution (frequency) of the distance of m6A peak summits to the closest given anchor point 5′ SJ (C), 3′ SJ (D), start codon (E), and stop codon (F) for nascent RNA (TNT-seq) and mRNA (m6A-seq; Schwartz et al., 2014).

See also Figure S1.

data (Schwartz et al., 2014) and called m6A peaks using the same pipeline. The majority of steady-state mRNA m6A peaks reside in the CDS (52%), 3′ UTR (28%), and 5′ UTR (12%), while only a minor fraction (4%) is intronic (Figure S1D). Almost half of the CDS-associated nascent m6A peaks reside within 100 nt upstream of the 5′ SJ, and approximately one-fifth are within 100 nt downstream of the 3′ SJ (Figure S1C). For steady-state mRNA, only 17% and 11% of the CDS peaks are within the respective intervals, suggesting a transient functional role of early m6A deposition (Figure S1D). By normalizing the number of m6A peaks to the length of the analyzed intervals and the respective input read coverage, we find that the early m6A deposition is enriched within 100 nt of the 5′ SJ exonic boundary (Figure 1A). To validate the early m6A sites, we assessed the presence of the m6A consensus DRACH motif by performing *de novo* motif search with HOMER (Heinz et al., 2010) in the regions ±150 nt around the peak summit of the top scoring peaks (score >20, n = 5,651) or in randomly generated 300-nt genomic intervals. We find a DGACH motif with a positional enrichment around the peak summit, in particular for exonic peaks (Figure 1B). We also identify three additional motifs sharing an SAG core, with a strong positional enrichment around the peak summit, especially for intronic peaks (Figure 1B). Early m6A deposition is predominant at and in close proximity to SJs (Figures 1C and 1D). In contrast, the picture is inversed around start and stop codons, with a relatively greater number of peaks in steady-state mRNA (Figures 1E and 1F). This finding led us to examine whether early m6A deposition in close proximity to SJs has an impact on splicing of RNA.

m6A Signatures Separate Distinct Intron Classes

To determine the splicing kinetics of newly transcribed RNA, we used BrU-Chase Seq as described previously (Louloupi et al., 2017; Paulsen et al., 2013). Cells were labeled with a 15-min BrU pulse and chased for 0, 15, 30, and 60 min, followed by RNA purification. To determine SE across all time points, we calculated the splicing index value θ (Mukherjee et al., 2017) (Figure 2A), yielding 13,532 introns with an extracted θ value ranging from 0 (unspliced) to 1 (fully spliced). The degree of splicing at 0 min, representing nascent RNA, is lower compared to steady-state chromatin-associated RNA (Conrad et al., 2014), indicating that nascent pre-mRNA is more efficiently captured by our approach than by chromatin fractionation (Figure 2B). Using k-means clustering, we called three clusters of distinct SE dynamics (SED; Experimental Procedures) representing 4,882 fast-, 5,702 medium-, and 2,948 slow-processed introns (Figures 2C–2F). Three representative cases are depicted in Figure 2E. We plotted the average m6A signal per nucleotide position around 5′ and 3′ SJs (Figures 2G–2H) and within length-binned introns for the three groups (Figure S2B). Strikingly, we find that fast-processed introns show greater m6A deposition at SJs, with an overall positive relationship between m6A deposited at 5′ and 3′ SJ exonic boundaries and processing efficiency (Figures 2G–2J and Figures S2A–S2C). By plotting the average frequency of m6A peak summits per nucleotide position (instead of the average m6A signal) for the three subgroups, we reach the same conclusion (Figures S2D–S2F). In contrast, slowly processed introns are associated with increased m6A deposition within the intron (Figures S2B and S2E). To address whether the position of an intron affects m6A signal and SE, we looked at the average m6A signal per nucleotide position around the 5′ and 3′ SJs of only the first and last introns (of transcripts with at least four exons), showing that the effect is independent of the position of the intron (Figures S2G–S2J).

m6A Deposition at Nascent RNA Predicts SED

To further investigate the impact of m6A deposition on nascent RNA in shaping the SED, we used a logistic regression model fit to predict fast- versus slow-processed introns (Figures 2I and 2J). We find that inclusion of the m6A at SJs as an additional parameter improves the predictive power of the model (Figure 2I), with the m6A contribution in predicting fast processing being comparable to other previously shown features, such as the 5′ and 3′ SJ sequence scores and distance to transcription start site (TSS) and transcription end site (TES) (Figure 2J) (Mukherjee et al., 2017). Intron length and internal m6A signal are significantly associated with slow processing (Figure 2J). To complement this analysis, we applied linear regression to predict SED as a continuous value (Figure S3). Again, introducing the m6A at SJs improves the correlation between predicted and measured SED (Figures S3A–S3C), further confirming the impact of early m6A deposition on RNA processing.

Intronic m6A Deposition Associates with Alternative Splicing

We assessed alternative versus constitutive splicing (by extracting the ψ value), as slow pre-mRNA processing has been shown to favor the occurrence of alternative splicing (Mukherjee et al., 2017) (Figure 2A). Alternative splicing events are significantly enriched in slow processed introns (odds ratio, 3.84; Fisher's exact test p value < 2.2e-16) (Figure 3A). Additionally, intronic m6A peaks are associated with upstream or downstream exon skipping approximately two times more often than expected by random chance (odds ratio, 1.7; Fisher's exact test p value < 2.2e-16), suggesting that intronic m6A deposition is involved in alternative splicing. In concurrence, the average m6A signal is greater along alternative versus constitutively spliced introns and the average m6A signal is greater at constitutive versus alternatively spliced SJ exonic boundaries (Figures 3B–3D). The overall intronic m6A, along with the intron length, are significant contributors in determining alternative splicing (Figure 3E). In contrast, m6A at SJ exonic boundaries and strong splice site consensus sequences (SJ score) ensure constitutive splicing (Figure 3E). Inclusion of m6A improves the predictive power of the model fit of constitutive versus alternative splicing (Figure 3F).

Splicing Factors Coincide with m6A Deposition

To investigate how m6A functionality in splicing is mediated, we analyzed available crosslinking immunoprecipitation sequencing (CLIP-seq) data for SRSF factors with an established role in splicing (Xiao et al., 2016). We find that both SRSF3 and SRSF10 show a high probability to have an m6A peak summit in close proximity (<250 nt) (Figures S4A and S4B), with SRSF10 showing relatively greater affinity (Figure S4C). The SAG motif core that we identify in early m6A peaks is reminiscent of the SRSF binding site motifs (Ajiro et al., 2016; Xiao et al., 2016). In addition, both SRSF3 and SFRF10 have been shown to bind near m6A, and while SRSF3 binding is augmented through interaction with YTHDC1, SRSF10 can bind independently to m6A modified regions (Xiao et al., 2016). In agreement with this observation, we find that the ratio of SRSF10/SRSF3 binding is greater at the SJ exonic boundaries for fast-processed introns and internally along within slow-processed introns (Figures S4D–S4F), in concordance with the respective relative enrichment of early m6A deposition (Figures 2G, 2H, and S2). The average ratio of SRSF10/SRSF3 binding clearly separates alternative and constitutive spliced introns (Figures S4G–S4I), most prominently along length-binned introns (Figure S4H). This result is in agreement with the observation that alternative splicing can be antagonistically regulated by SRSF10 versus SRSF3 binding (Xiao et al., 2016). These results suggest that m6A could play a role in shaping the final outcome of splicing through the recruitment of splicing factors with varying m6A affinities.

qTNTchase-Seq Identifies m6A-Marked Fast-Track RNAs

To separate direct m6A-mediated effects on RNA processing from sequence specific ones, we used qTNTchase-seq. Here, BrU-labeled RNA was isolated at 0 and 30 min chase and m6A transcripts were isolated with an m6A-specific antibody without fragmentation. Both supernatant (m6A negative transcripts) and eluate (m6A positive transcripts) were sequenced for each time point to obtain quantitative information, and we calculated the

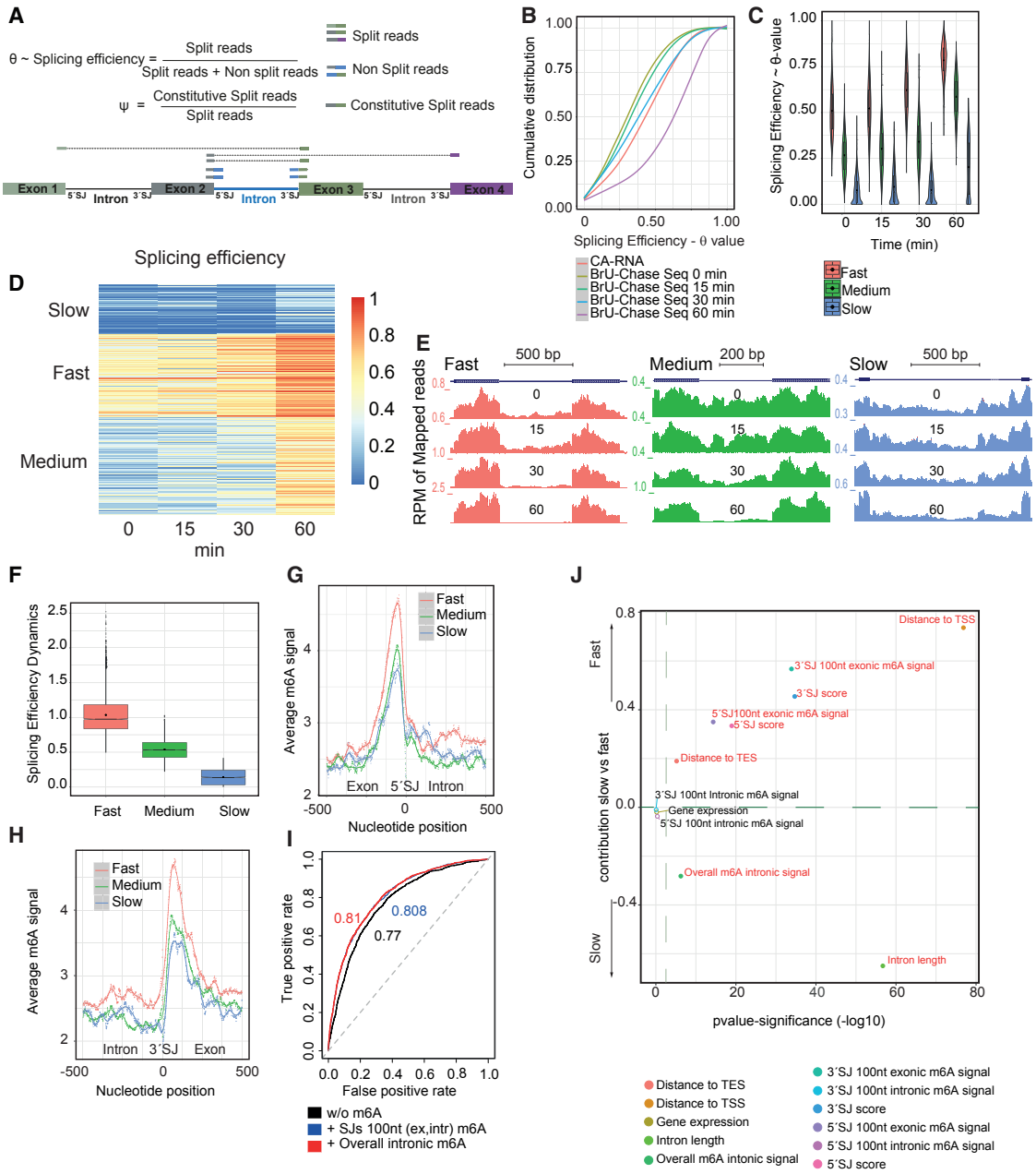

Figure 2. m6A Deposition at Nascent RNA Determines SED

(A) Definition of θ and ψ value.

(B) Cumulative distribution of the SE index from chromatin-associated RNA-seq (Conrad et al., 2014), BrU-Chase Seq (0, 15, 30, and 60 min).

(C) Violin plot representing the density of the SE index (θ value) distribution with embedded box and whisker plots for introns grouped on the basis of differential splicing kinetics.

(D) Heatmap showing the k-means clustering results (with k = 3) of the splicing SE index (θ value) of the 13,532 filtered introns measured for the BrU-Chase time points. Introns are clustered into fast, medium, and slow processed.

(E) UCSC genome browser views of representative cases of introns from each of the three clustering groups.

(F) Boxplot showing distribution of the SED for the fast-, medium-, and slow-processed intron groups.

(G and H) Average m6A signal per nucleotide position in a ±500-nt window around 5′ SJs (G) and 3′ SJs (H) of the filtered introns.

(I) Average receiver-operating characteristic (ROC) curve for discrimination of fast versus slow introns, including all characteristics and excluding m6A. The respective area under the curve (AUC number) is indicated.

(J) Contribution of each feature to the model fit of fast versus slow processing calculated as the coefficients from the binary logistic regression with the associated estimated significance (−log10 p value). The features with p value < 0.001 are colored red.

See also Figures S2–S4.

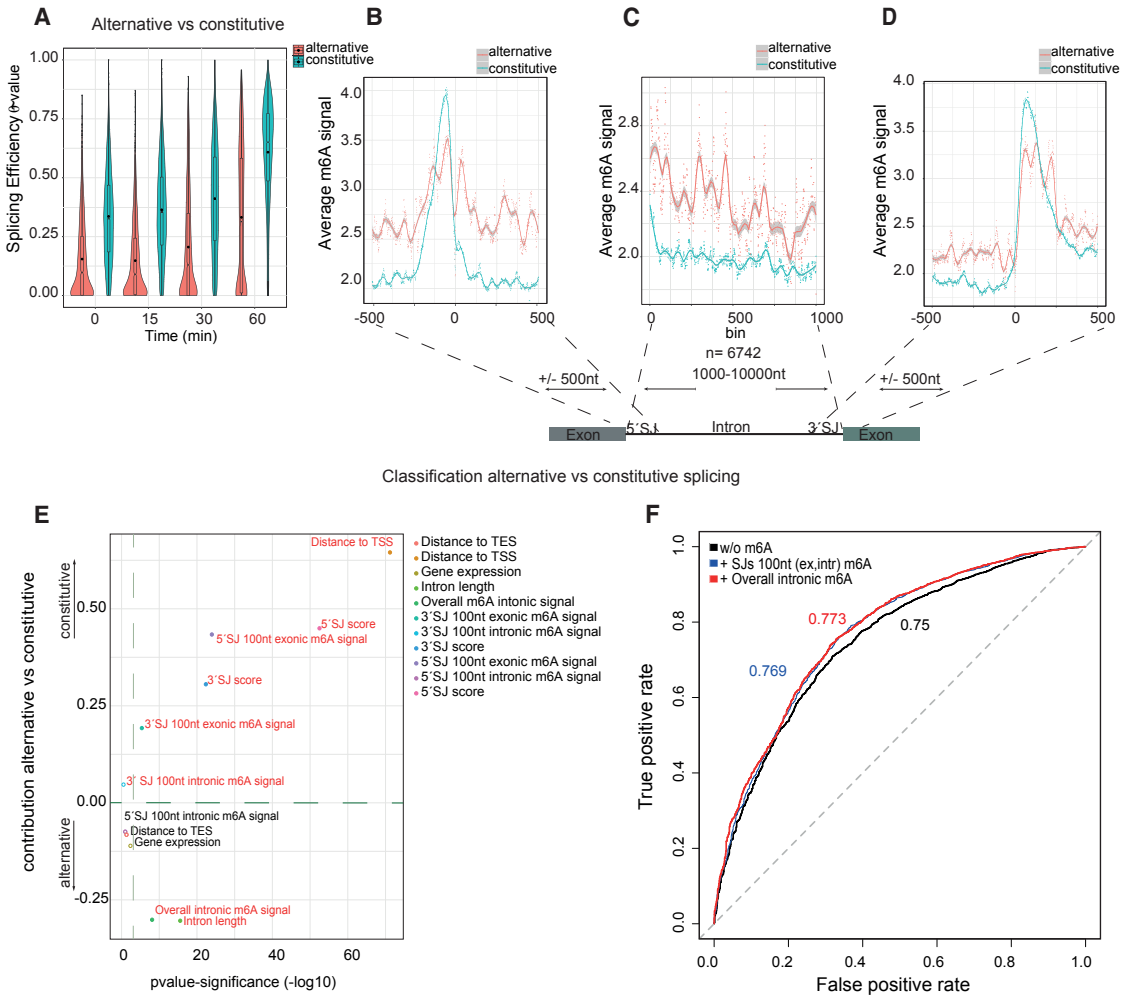

Figure 3. Intronic m6A Deposition Associates with Alternative Splicing

(A) Violin plots showing density of the distribution (with embedded box-and-whiskers plots) of θ value for introns classified as either constitutive or alternative spliced extracted from all pulse-chase time points.

(B–D) Average m6A signal per nucleotide position in a ±500-nt window around the 5′ SJ (B) and 3′ SJ (D) and per bin (C) of 6,742 introns with length 1,000–10,000 nt. The average m6A signal is extracted separately for the two subgroups (constitutive and alternative). The lines represent LOESS curve fitting (local polynomial regression), with the 95% confidence interval shaded gray.

(E) The contribution of each feature to alternative versus constitutive splicing, calculated as the coefficients of the binary logistic regression fit with associated estimated significance (−log10 p value). Features with $p < 0.001$ are colored red.

(F) Average ROC for the logistic regression prediction of the alternative versus constitutive splicing using all features, with and without m6A data. The respective AUC number is indicated.

See also Figure S4.

m6A level per transcript (Molinie et al., 2016). On a transcriptome-wide scale, we observe a strong concordance of m6A levels between biological replicates, both for the top 25% expressed transcripts and for all transcripts with non-zero coverage (0 min: Pearson $r = 0.89$, p value < 2.2e-16; 30 min: Pearson $r = 0.91$, p value < 2.2e-16). The m6A levels do not significantly differ between 0 and 30 min chase, indicating that the overall m6A modification levels of transcripts remain the same for at least ~45 min after transcription (not shown). To follow SE, we extracted the transcript splicing index from m6A-positive and m6A-negative transcripts at 0 and 30 min chase. Within the pulse, corresponding to a 15-min window of transcription, m6A-positive transcripts show significantly higher SE than m6A-negative transcripts (Figure 4A). In addition, by measuring SED at the transcript level, we find that the m6A-positive transcripts show significantly greater processing than their m6A-negative counterparts (two tailed paired *t test* p value < 2.2e-16) (Figure 4B). Importantly, processing appears significantly enhanced for the m6A fraction of individual transcripts; ~76% show gain of SED in the m6A fraction, revealing a direct and sequence-independent impact of m6A on processing kinetics (Figure 4C). We further examined the SE locally for the 13,532

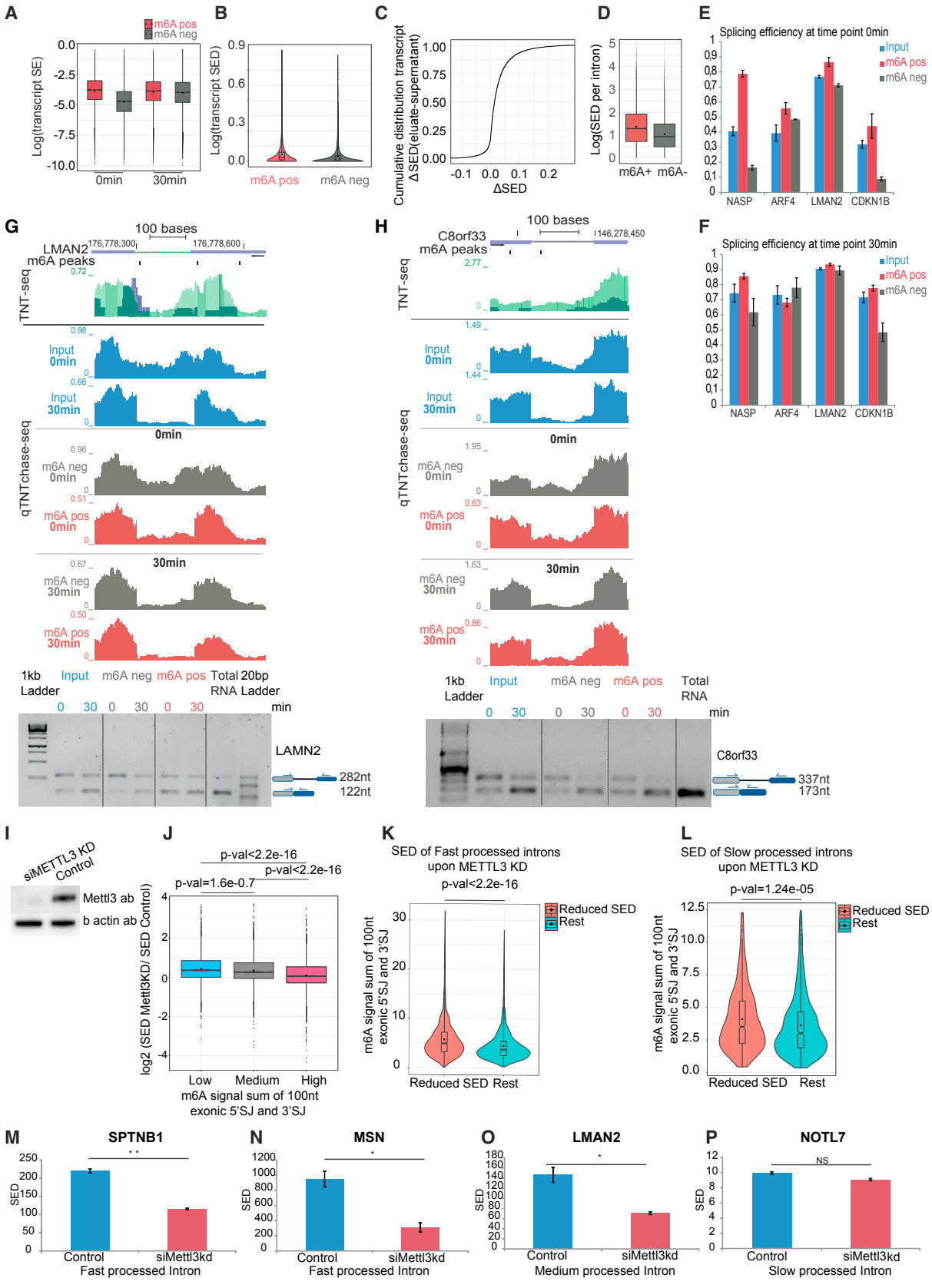

(legend on next page)

filtered introns. We find that ~14% have significantly higher SE in the m6A-positive transcripts and show a 1.26-fold enrichment over random chance to have an m6A peak in the 5′ SJ 250-nt exonic boundary (odds ratio, 1.265; Fisher's exact test *p* value = 0.0006745). In addition, individual intron loci show on average significantly higher SED in the m6A-positive versus m6A-negative transcripts (two-tailed paired t test p value < 2.2e-16) (Figure 4D).

We used qPCR to analyze the splicing kinetics of four candidate SJs that have at least one m6A peak (±250 nt). Strikingly, at time point 0, m6A-positive transcripts show higher SE than the m6A-negative transcripts (Figures 4E and 4F). We confirmed this result with semiquantitative PCR (Figures 4G and 4H).

Nascent m6A Effects Are METTL3 Dependent

To provide a direct link between RNA splicing kinetics and m6A deposition at SJs, we assessed the splicing kinetics after METTL3 knockdown (METTL3 KD) (60 min chase) (Figure 4I). The intron dataset was divided into three equal-size quantiles based on the m6A signal at 5′ and 3′ SJs (5′ and 3′ SJ 100-nt exonic intervals), and the SED was calculated. We plotted the log2 ratio of SED for METTL3 KD to control for introns with low, medium, and high m6A signal (Figure 4J). For introns with high m6A signal on both 5′ and 3′ SJs, we observe a decreased SED upon METTL3 KD for approximately half of the entries (log2 SED ratio METTL3 KD/control < 0) (Figure 4J). For introns with low and medium m6A signal (log2 SED ratio METTL3 KD/control > 0), we observe an increased SED (Figure 4J). The difference in the SED ratio (log2 METTL3 KD/control) of high m6A signal compared to low or medium is significant for both comparisons (t test p value < 2.2e-16). We then focused on fast-processed introns and plotted the m6A signal (sum of 5′ SJ and 3′ SJ 100-nt exonic area) for those that show reduced SED upon METTL3 KD versus the rest (Figure 4K). We find that the METTL3-affected introns have significantly higher m6A at the 5′ and 3′ SJ exonic boundaries. This verifies that the 5′ and 3′ SJ exonic methylation promotes fast splicing kinetics, as also shown by the logistic regression model fit (Figure 2J). We see the same but less pronounced tendency for the slow-processed introns (Figure 4L). qPCR analysis of SED for four candidates confirms the transcriptome-wide data (Figures 4M–4P).

DISCUSSION

We identify an enrichment of m6A deposition near the 5′ SJs of nascent RNA transcripts, and we show that early m6A deposition is associated with distinct RNA processing kinetics. Most importantly, we compare the processing of individual m6A-positive transcripts versus their m6A-negative counterparts, demonstrating that m6A directly controls splicing kinetics irrespectively of the underlying transcript sequence. Our findings suggest that m6A serves as a labeling signal that could be recognized by m6A reader proteins to destine methylated transcripts for specific splicing kinetics. This is in agreement with a study describing m6A methylation as a mark for selective nuclear processing, providing evidence for an m6A-dependent mRNA metabolism (Roundtree et al., 2017).

Our findings furthermore reveal that intronic m6A peaks are enriched in introns involved in alternative splicing. The m6A demethylase FTO binds mostly to introns and mediate removal of m6A. Knockout of FTO causes alternative splicing events with a preference for exon skipping, suggesting that demethylation of mRNA transcripts promotes exon inclusion under normal conditions (Bartosovic et al., 2017). Taken together, these findings suggest that intronic m6A marks that are not targeted or not yet removed by FTO mediate exon skipping, while introns involved in constitutive splicing show no enrichment in the m6A signal and most probably are targets of FTO (Bartosovic et al., 2017). In mRNAs, m6A is enriched in the consensus DRACH motif; however, not all DRACH motifs are methylated, indicating that the presence of the sequence motif alone is not enough to drive m6A deposition. FTO CLIP data show no significant enrichment of the DRACH motif (Bartosovic et al., 2017), leading us to hypothesize that early intronic m6A deposition is mostly in non-DRACH sequences where FTO can detect and eventually remove the m6A marks.

Recently, the m6A reader YTHDC1 was shown to recruit SRSF3 while competing away SRSF10. YTHDC1 binds m6A sites and promote exon inclusion (Xiao et al., 2016). In the absence of YTHDC1 and SRSF3, SRSF10 has the availability to bind to free m6A sites independently, promoting exon skipping. SRSF3 knockdown in U2OS cells has also been shown to cause exon-skipping events (Ajiro et al., 2016). Using *de*

Figure 4. qTNTchase-Seq Identifies m6A-Marked Fast-Track RNAs

(A) Boxplot representing the overall SE of methylated (m6A positive) versus non-methylated (m6A negative) transcripts at time points 0 and 30 min.

(B) Violin plots showing distribution of the transcript SED in m6A-positive and m6A-negative fractions (two-tailed Student's t test p value < 2.2e-16).

(C) Cumulative distribution of transcript SED differences between the methylated and unmethylated state (⊿SED = SED m6A positive − SED m6A negative).

(D) Boxplot displaying SED per intron in m6A-positive and m6A-negative transcripts (two-tailed paired t test p value < 2.2e-16).

(E and F) qPCR analysis of the local intronic SE of methylated versus non-methylated transcripts for 0 min (E) and 30 min (F).

(G and H) UCSC genome browser tracks of qTNTchase-seq data for LMAN2 (G) and C8orf33 (H) representing the transcript regions used for the qRT-PCR analysis. Normalized read coverage (reads per million of total number of mapped reads) tracks for input (blue), supernatant m6A negative (gray), and eluate m6A positive (pink). The upper overlay track represents the TNT-seq with purple for input and green for IP; black rectangles above represent the called m6A peaks. Below tracks for each sample are agarose gels depicting semiquantitative PCR of input, m6A-positive, and m6A-negative samples for 0 and 30 min.

(I) Western blot for METTL3 KD.

(J) Log2 ratio of SED in METTL3 KD to control for introns with low, medium, and high m6A signal at both 5′ and 3′ SJs (100-nt exonic area).

(K) m6A signal at both 5′ SJs and 3′ SJs (100 nt exonic area) for the fast-processed introns that show reduced SED in the METTL3 KD condition versus the rest (two-tailed Student's t test p value < 2.2e-16).

(L) m6A signal at both 5′ SJs and 3′ SJs (100 nt exonic area) for the slow-processed introns that show reduced SED in the METTL3 KD condition versus the rest (two-tailed Student's t test p value < 2.2e-16).

(M–P) qPCR analysis of SED for fast- (M and N), medium- (O), and slow-processed (P) introns (error bars show SD, n = 2 biological replicates (*p < 0.05 and **p < 0.01, two-tailed Student's t test).

novo motif analysis, we identify three additional motifs sharing a SAG core reminiscent of the SRSF binding site consensus, suggesting that m6A could be involved in recruiting splicing factors to control SE and alternative splicing.

The lack of strong consensus sequences at SJs of many introns may be compensated by the presence of m6A that could eventually attract splicing factors to exert their function. Our study shows that the crucial role of m6A on SED as well as on alternative splicing is position dependent. m6A deposited in intronic regions sort transcripts to a slow-track processing pathway and is associated with alternative splicing while m6A deposited at exonic boundaries of SJs sort transcripts to a fast-track processing pathway and constitutive splicing.

EXPERIMENTAL PROCEDURES

Cell Culture and BrU-Chase Sequencing

HEK293 cells were cultured in DMEM growth medium supplemented with 10% fetal bovine serum (FBS) under normal growth conditions (37°C and 5% CO_2). Cells were 70%–80% confluent before addition of BrU. BrU (−5-bromouridine, Santa Cruz Biotechnology catalog number CAS 957-75-5) was added to a final concentration of 2 mM to the medium and cells were incubated at normal growth conditions for 15 min. Cells were washed three times in PBS and either collected directly or chased in conditional medium supplemented with 20 mM uridine (Sigma catalog number U3750-25G) for 15, 30, and 60 min. RNA was purified using TRIzol following the manufacturer's instructions.

TNT-Seq

For one TNT-seq sample, ~25 150-mm plates were used for BrU labeling. RNA was labeled and isolated as described above. RNA concentration was adjusted to 2 μg/μL with nuclease-free water. 18 μL RNA was added to a thin-walled 200-μl PCR tube following the addition of 2 μL 10X fragmentation mixture (100 mM Tris-HCl [pH 7.4] and 100 mM $ZnCl_2$ in nuclease-free water). Distribution of post-fragmentation size (~100 nt) was analyzed using an Agilent 2100 Bioanalyzer with an Agilent RNA 6000 Pico kit according to the manufacturer's instructions. 400–600 μg fragmented BrU-labeled total RNA was used for each BrU immunoprecipitation (IP). BrU-RNA isolation was performed as described above. 5 μg BrU fragmented RNA was used as input for the m6A-IP buffer. An RNA-antibody-beads mixture was incubated for 2 hr at 4°C with gentle rotation in a final volume of 0.8 mL in protein low-binding tubes. Three washing steps were performed with 1X m6A-IPbuffer (1st and 2nd wash) and high-salt m6A-IP buffer (500 mM NaCl, 0.1% Igepal CA-6300, 10 mM Tris-HCl [pH 7.5]) (3rd wash). At the last wash, the protein low-binding tubes were replaced with DNA LoBind tubes. For elution, 80 μL elution buffer (1X m6A-IP buffer + 6.7 mM m6A nucleotides) was added directly on the beads, and the tubes were incubated for 1 hr with continuous shaking (1,100 rpm) at 4°C. After the second round of elution, RNA was ethanol precipitated and resuspended in 15 μL RNase-free water, and the RNA concentration was measured using the Qubit RNA HS Assay Kit as per the manufacturer's instructions.

siRNA Transfection

HEK293 cells were transfected with four different siRNAs targeting METTL3 transcript (Table S1) using HiPerFect Transfection Reagent from QIAGEN. In brief, reverse transfection was performed using 1×10^6 cells for a single 100-mm plate. Cells were seeded in a final 4 mL volume of medium without antibiotics. 12 μL transfection reagent together with siRNAs (25 nM final concentration) was incubated at room temperature (RT) in 1 mL Opti-MEM I Reduced Serum Medium after mixing for 20 min. The transfection complexes were added drop-wise into the plate. 16 hr after transfection, 5 mL cell culture medium was added to each plate. A second transfection was performed 24 hr after the first transfection. After 40 hr, 5 mL cell culture medium was added to each plate. Knockdown efficiency was analyzed with western blot (anti-METTL3 polyclonal antibody; Protein Tech catalog number 15073-1-AP). BrU-Chase Seq samples were prepared 72 hr after the first transfection. The experiments were performed in duplicate.

RNA Sequencing and Data Analysis

For the BrU- Chase Seq, the library preparation was done using the TrueSeq Stranded Total RNA Kit (Illumina). Sequencing was performed on an Illumina HiSeq 2500 instrument to obtain ~200 million reads per sample. For the TNT-Seq, 100 ng of Input BrU-labeled fragmented RNA and 100 ng of TNT-IP eluate RNA were subjected to library preparation following the TruSeq Stranded mRNA Library Preparation Kit instructions with some modifications.

DATA AND SOFTWARE AVAILABILITY

The accession numbers for the BrU-chase-seq, TNT-seq, qTNTchase-seq, and METTL3 KD BrU-chase-seq data reported in this paper are GEO: GSE92565 and GSE83561.

SUPPLEMENTAL INFORMATION

Supplemental Information includes four figures and one table and can be found with this article online at https://doi.org/10.1016/j.celrep.2018.05.077.

ACKNOWLEDGMENTS

E.N. has been funded by a postdoctoral stipend from the Alexander von Humboldt Foundation. Work in the author's laboratory is funded by the German Research Council (DFG), the Alexander von Humboldt Foundation (Sofja Kovalevskaja Award), and the Novo Nordisk Foundation (Hallas Møller Investigator) to U.A.V.Ø.

AUTHOR CONTRIBUTIONS

Conceptualization, A.L., E.N., T.C., and U.A.V.Ø.; Methodology, A.L., E.N., T.C., and U.A.V.Ø.; Investigation, A.L. and E.N.; Validation, A.L; Formal Analysis, Data Curation, Software, E.N.; Writing – Original Draft, Visualization, A.L, E.N., and U.A.V.Ø.; Writing – Review & Editing, A.L., E.N., T.C., and U.A.V.Ø.; Supervision, Funding Acquisition, U.A.V.Ø.

DECLARATION OF INTERESTS

The authors declare no competing interests.

Received: January 10, 2018
Revised: April 30, 2018
Accepted: May 23, 2018
Published: June 19, 2018

REFERENCES

Ajiro, M., Jia, R., Yang, Y., Zhu, J., and Zheng, Z.-M. (2016). A genome landscape of SRSF3-regulated splicing events and gene expression in human osteosarcoma U2OS cells. Nucleic Acids Res. *44*, 1854–1870.

Bartosovic, M., Molares, H.C., Gregorova, P., Hrossova, D., Kudla, G., and Vanacova, S. (2017). N6-methyladenosine demethylase FTO targets pre-mRNAs and regulates alternative splicing and 3′-end processing. Nucleic Acids Res. *45*, 11356–11370.

Conrad, T., Marsico, A., Gehre, M., and Orom, U.A. (2014). Microprocessor activity controls differential miRNA biogenesis In Vivo. Cell Rep. *9*, 542–554.

Dominissini, D., Moshitch-Moshkovitz, S., Schwartz, S., Salmon-Divon, M., Ungar, L., Osenberg, S., Cesarkas, K., Jacob-Hirsch, J., Amariglio, N., Kupiec, M., et al. (2012). Topology of the human and mouse m6A RNA methylomes revealed by m6A-seq. Nature *485*, 201–206.

Fu, Y., Dominissini, D., Rechavi, G., and He, C. (2014). Gene expression regulation mediated through reversible m^6A RNA methylation. Nat. Rev. Genet. *15*, 293–306.

Harcourt, E.M., Kietrys, A.M., and Kool, E.T. (2017). Chemical and structural effects of base modifications in messenger RNA. Nature *541*, 339–346.

Heinz, S., Benner, C., Spann, N., Bertolino, E., Lin, Y.C., Laslo, P., Cheng, J.X., Murre, C., Singh, H., and Glass, C.K. (2010). Simple combinations of lineage-determining transcription factors prime cis-regulatory elements required for macrophage and B cell identities. Mol. Cell *38*, 576–589.

Jia, G., Fu, Y., Zhao, X., Dai, Q., Zheng, G., Yang, Y., Yi, C., Lindahl, T., Pan, T., Yang, Y.-G., and He, C. (2011). N6-methyladenosine in nuclear RNA is a major substrate of the obesity-associated FTO. Nat. Chem. Biol. *7*, 885–887.

Ke, S., Pandya-Jones, A., Saito, Y., Fak, J.J., Vågbø, C.B., Geula, S., Hanna, J.H., Black, D.L., Darnell, J.E., Jr., and Darnell, R.B. (2017). m^6A mRNA modifications are deposited in nascent pre-mRNA and are not required for splicing but do specify cytoplasmic turnover. Genes Dev. *31*, 990–1006.

Liu, J., Yue, Y., Han, D., Wang, X., Fu, Y., Zhang, L., Jia, G., Yu, M., Lu, Z., Deng, X., et al. (2014). A METTL3-METTL14 complex mediates mammalian nuclear RNA N6-adenosine methylation. Nat. Chem. Biol. *10*, 93–95.

Liu, N., Dai, Q., Zheng, G., He, C., Parisien, M., and Pan, T. (2015). N(6)-methyladenosine-dependent RNA structural switches regulate RNA-protein interactions. Nature *518*, 560–564.

Liu, N., Zhou, K.I., Parisien, M., Dai, Q., Diatchenko, L., and Pan, T. (2017). N6-methyladenosine alters RNA structure to regulate binding of a low-complexity protein. Nucleic Acids Res. *45*, 6051–6063.

Louloupi, A., Ntini, E., Liz, J., and Ørom, U.A. (2017). Microprocessor dynamics shows co- and post-transcriptional processing of pri-miRNAs. RNA *23*, 892–898.

Meyer, K.D., Patil, D.P., Zhou, J., Zinoviev, A., Skabkin, M.A., Elemento, O., Pestova, T.V., Qian, S.B., and Jaffrey, S.R. (2015). 5′ UTR m(6)A promotes cap-independent translation. Cell *163*, 999–1010.

Molinie, B., Wang, J., Lim, K.S., Hillebrand, R., Lu, Z.X., Van Wittenberghe, N., Howard, B.D., Daneshvar, K., Mullen, A.C., Dedon, P., et al. (2016). m(6)A-LAIC-seq reveals the census and complexity of the m(6)A epitranscriptome. Nat. Methods *13*, 692–698.

Mukherjee, N., Calviello, L., Hirsekorn, A., de Pretis, S., Pelizzola, M., and Ohler, U. (2017). Integrative classification of human coding and noncoding genes through RNA metabolism profiles. Nat. Struct. Mol. Biol. *24*, 86–96.

Narayan, P., and Rottman, F.M. (1988). An in vitro system for accurate methylation of internal adenosine residues in messenger RNA. Science *242*, 1159–1162.

Paulsen, M.T., Veloso, A., Prasad, J., Bedi, K., Ljungman, E.A., Tsan, Y.C., Chang, C.W., Tarrier, B., Washburn, J.G., Lyons, R., et al. (2013). Coordinated regulation of synthesis and stability of RNA during the acute TNF-induced proinflammatory response. Proc. Natl. Acad. Sci. USA *110*, 2240–2245.

Ping, X.-L., Sun, B.-F., Wang, L., Xiao, W., Yang, X., Wang, W.-J., Adhikari, S., Shi, Y., Lv, Y., Chen, Y.-S., et al. (2014). Mammalian WTAP is a regulatory subunit of the RNA N6-methyladenosine methyltransferase. Cell Res. *24*, 177–189.

Roundtree, I.A., Luo, G.-Z., Zhang, Z., Wang, X., Zhou, T., Cui, Y., Sha, J., Huang, X., Guerrero, L., Xie, P., et al. (2017). YTHDC1 mediates nuclear export of N^6-methyladenosine methylated mRNAs. eLife *6*, e31311.

Schwartz, S., Mumbach, M.R., Jovanovic, M., Wang, T., Maciag, K., Bushkin, G.G., Mertins, P., Ter-Ovanesyan, D., Habib, N., Cacchiarelli, D., et al. (2014). Perturbation of m6A writers reveals two distinct classes of mRNA methylation at internal and 5′ sites. Cell Rep. *8*, 284–296.

Slobodin, B., Han, R., Calderone, V., Vrielink, J.A.F.O., Loayza-Puch, F., Elkon, R., and Agami, R. (2017). Transcription impacts the efficiency of mRNA translation via co-transcriptional N6-adenosine methylation. Cell *169*, 326–337.e12.

Wang, X., Lu, Z., Gomez, A., Hon, G.C., Yue, Y., Han, D., Fu, Y., Parisien, M., Dai, Q., Jia, G., et al. (2014). N6-methyladenosine-dependent regulation of messenger RNA stability. Nature *505*, 117–120.

Xiao, W., Adhikari, S., Dahal, U., Chen, Y.-S., Hao, Y.-J., Sun, B.-F., Sun, H.-Y., Li, A., Ping, X.-L., Lai, W.-Y., et al. (2016). Nuclear m(6)A reader YTHDC1 regulates mRNA splicing. Mol. Cell *61*, 507–519.

Xu, C., Wang, X., Liu, K., Roundtree, I.A., Tempel, W., Li, Y., Lu, Z., He, C., and Min, J. (2014). Structural basis for selective binding of m6A RNA by the YTHDC1 YTH domain. Nat. Chem. Biol. *10*, 927–929.

Zheng, G., Dahl, J.A., Niu, Y., Fedorcsak, P., Huang, C.M., Li, C.J., Vågbø, C.B., Shi, Y., Wang, W.L., Song, S.H., et al. (2013). ALKBH5 is a mammalian RNA demethylase that impacts RNA metabolism and mouse fertility. Mol. Cell *49*, 18–29.

Cell Reports, Volume *23*

Supplemental Information

Transient N-6-Methyladenosine Transcriptome Sequencing Reveals a Regulatory Role of m6A in Splicing Efficiency

Annita Louloupi, Evgenia Ntini, Thomas Conrad, and Ulf Andersson Vang Ørom

Supplemental Experimental Procedures

Cell culture and BrU-chase Seq.

HEK293 cells were cultured in DMEM growth-medium supplemented with 10% Fetal Bovine Serum (FBS) under normal growth conditions (37°C and 5% CO_2). The day before bromouridine (BrU) labelling ~2.0 x 10^6 cells were seeded in 100 mm plates with 10ml media, one plate for each time point. Cells were 70-80% confluent before the addition bromouridine (BrU). BrU (-5-Bromouridine cat.no. CAS 957-75-5 Santa Cruz Biotechnology) was added to a final concentration of 2 mM to the media and cells were incubated at normal growth conditions for 15 min (pulse). Cells were washed three times in PBS and either collected directly (0 min chase time point) or chased in conditional media supplemented with 20 mM uridine (Sigma cat.no U3750-25G) for 15, 30 and 60 min. RNA was purified using TRIzol following manufacturer's instructions.

In the next step we followed the protocol of (Paulsen et al., 2013) with some modifications.

40ul of anti of anti-mouse IgG magnetic Dynabeads (Invitrogen) were transferred to a 1.5ml microfuge Protein Low binding tube and washed 3 times with BrU-IP 1X buffer (0.1% BSA in RNAse free PBS). After the final wash, the beads were resuspended in BrU-IP 1X buffer supplemented with SUPERase• In™ RNase Inhibitor 1:2000 together with BrdU antibody (5µg of antibody per 100 µg RNA). Antibody-beads mixture was incubated for 1 hour at room temperature with gentle rotation following 3 washes with 1X BrU-IP. 150 µg RNA was used for each BrU-IP and heated up for 4 min at 65°C prior to IP. The same amount of unlabeled total RNA was used as a negative control. 5X BrU-IP (0.5% BSA 5X PBS supplemented with SUPERase• In™ RNase Inhibitor 1:2000) was added to the RNA to a final concertation of 1X. RNA-antibody-beads mixture was incubated for 90 min at room temperature with gentle rotation in a final volume of 800 ul. The beads were washed three times with 800 ul 1X BrU-IP at room temperature. For all wash steps, with the exception of the elution step, the beads were washed for 5 min rotating then placed on a magnetic rack and the wash buffers were

discarded. At the last wash the Protein low binding tubes were replaced with DNA LoBind tubes. For elution 200 ul of Elution buffer (0.1% BSA and 25 mM bromouridine in PBS) were added directly on the beads and the tubes were incubated for 60 min with continuous shaking (1100 rpm) at 4 °C. The supernatant (eluate w/o beads) was transferred to a new tube and RNA was precipitated by adding 1/10 volumes of 3M sodium acetate (pH 5.2) and 3-4 volumes of 100% ethanol. RNA was allowed to precipitate at −80 °C overnight. RNA pellet was washed twice with 75% ethanol and resuspended in RNase-free water. RNA quality was analyzed using Agilent 2100 Bioanalyzer with an Agilent RNA 6000 Pico kit according to the manufacturer's instructions.

TNT-seq

For one TNT-seq sample ~25 150 mm plates were used for BrU labelling. RNA was metabolically labelled with BrU for 15 min and RNA was isolated as described above. RNA concentration was adjusted to 2 µg/ul with nuclease free water. 18 ul of RNA was added to thin-walled 200µl PCR tube following addition of 2 ul of 10X fragmentation mixture (containing 800 µl of RNase-free water, 100 µl of 1M Tris-HCl pH 7.4 and 100 µl 1M of $ZnCl_2$). After vortex and quick spinning the tubes were incubated in 94 °C for 3.5 min in a preheated thermal cycler block with the heated lid closed. Tubes were quickly removed from the thermocycler and placed on ice following addition of 2 µl of 0.5 M EDTA. After vortex and quick spin the RNA was collected in a tube to continue with for RNA precipitation using 1/10 volumes of 3 M sodium acetate (pH 5.2), 3-4 volumes of 100% ethanol. RNA was allowed to precipitate at −80 °C overnight. The following day tubes were centrifuged at full speed for 30 min at 4 °C. RNA pellet was washed twice with 75% ethanol and resuspended in 400-500 ul of RNase-free water. Validation of post fragmentation size (~100 nt) distribution was analyzed using Agilent 2100 Bioanalyzer with an Agilent RNA 6000 Pico kit according to the manufacturer's instructions. 400-600 ug fragmented BrU labeled total RNA was used

for each BrU-IP. BrU-RNA isolation was performed as described above. The BrU-IP recovery was approximately 0.09-0.16% of input. 4.5 ug of BrU fragmented RNA was used as input for the m6A immunoprecipitation. 40 ul of Dynabeads® Protein A (Invitrogen) per sample was transferred to a 1.5 ml microfuge Protein LoBind tube and washed 3 times with 1X m6A-IP (500 mM NaCl, 0.1% NP-40, 10 mM Tris-HCl, pH 7.5). After final wash the beads were resuspended in 800 ul 1X m6A-IP buffer supplemented with SUPERase• In™ RNase Inhibitor 1:1000. 1ug of affinity purified anti-m6A polyclonal antibody (Synaptic Systems) per 2.5 ug BrU-RNA was added to the beads and incubated for 60 min at room temperature with gentle rotation. As a negative control, we used Dynabeads® Protein A magnetic beads bound to an irrelevant IgG. Beads were washed 3 times with m6A-IP 1X buffer for 5 min on the rotator. 5 ug of BrU Fragmented RNA was used as input. RNA was heated up for 4 min at 65 °C. 5X m6A-IP buffer (50 mM Tris-HCl, 750 mM NaCl and 0.5% (vol/vol) Igepal CA-6300 supplemented with SUPERase• In™ RNase Inhibitor) was added to have the RNA in 1X m6A-IP buffer. RNA-antibody-beads mixture was incubated for 2 hours at 4°C with gentle rotation in a final volume of 0.8ml in Protein low binding tubes. Three washing steps followed using m6A-IP 1X buffer (1^{st} and 2^{nd} wash) and high salt m6A-IP buffer (500 mM NaCl, 0.1% Igepal CA-6300, 10 mM Tris-HCl, pH 7.5) (3^{rd} wash). For all wash steps, with the exception of the elution step, the beads were washed for 5 min then placed on a magnet and the wash buffers were discarded. At the last wash the Protein low binding tubes were replaced with DNA LoBind tubes. For elution 80 ul of Elution buffer (1X m6A-IP buffer + 6.7 mM m6A nucleotides) were added directly on the beads and the tubes were incubated for 1 hour with continuous shaking (1100 rpm) at 4 °C. The beads were spun down and the supernatant was transferred to a clean tube. After the second round of elution the eluted RNA was precipitated using ethanol precipitation as described above. RNA pellet was resuspended in 15 ul RNase-free water and using Qubit® RNA HS Assay Kit we measured the RNA concentration following manufacturer's instructions.

qTNTchase-seq, qPCR, RT-PCR.

RNA was metabolically labelled with BrU for 15 min and chased for 30 min as described above. RNA was purified using TRIzol following manufacturer's instructions. 200 ug total BrU labeled RNA was used as Input for the BrU-RNA isolation. After the elution step (200 ul of 0.1% BSA and 25mM bromouridine in PBS) we added 50 ul of 5X m6A-IP buffer. 4 ug (1 ug ab per 500 ng RNA) m6A ab were coupled to 40 ul Dynabeads® Protein A as described above, resuspended in 550 ul m6A-IP 1X buffer and added to the RNA mixture. RNA-antibody-beads mixture was incubated for 60 min at room temperature with gentle rotation. The supernatant was kept and RNA was isolated with TRIzol. The beads were washed 3 times for 5 min at RT (twice with low salt m6A-IP 1X buffer and last wash high salt m6A-IP 1X buffer). We eluted the RNA captured by m6A antibody by competition as described in TNT-Seq section. cDNA synthesis was performed using the same amount of RNA (10-20 ng) from all fractions (Input BrU-RNA 0 min, Input BrU-RNA 30 min chase, Supernatant m6A-negative 0 min, Supernatant m6A-negative 30 min chase, IP m6A-positive 0 min, IP m6A-positive 30 min chase). RT-PCR was performed using Q5 Hot Start High-Fidelity DNA Polymerase New England Biolabs with initial denaturation 98 °C 30s, then 32 cycles of 98 °C 10 s, 58 °C 20 s and 72 °C 55 s and final extension 72 °C 2 min. PCR products were resolved on agarose gel. Spike-in controls were *in vitro* transcribed using T7 RNA Polymerase Invitrogen following manufactures instructions. For the methylated transcripts N6-methyl-ATP (TriLink) was used in a ratio 4:1 to ATP in the *in vitro* transcription reaction. GFP and Luciferase sequences were used as template for the RNA transcription. For each qTNTchase-seq sample before m6A IP, *in vitro*–transcribed transcripts with and without m^6A modification were mixed into the samples as spike-in controls at the indicated percentage of m6A-modified to m6A-unmodified transcript (Molinie et al., 2016). For all samples after BrU-IP but before m6A-IP we added $2.5x10^7$ copies from each spike including: 0% GFP and

20% luciferase. Before the library preparation for sequencing, 1 ul of 1:2000 dilution of the universal ERCC spike-in control A (Invitrogen) was added to each fraction (100 ng).

siRNA transfection

HEK293 cells were transfected with four different siRNAs targeting METTL3 transcript (see Supplemetary Table 1) using HiPerFect Transfection Reagent from QIAGEN. In brief, reverse transfection was performed using 1 x 10^6 cells for a single 100 mm plate. Cells were seeded in a final 4 ml final volume of media without antibiotics. 12 ul of transfection reagent together with siRNAs (25 nM final concentration) were incubated at room temperature in 1 ml Opti-MEM^{TM} I Reduced Serum Media after mixing for 20 min. The transfection complexes were added dropwise into the plate. 16 hours after transfection 5 ml of cell culture media were added to each plate. 24 hours after the first transfection we performed a second hit using the same amount of transfection reagent and siRNAs as the first round. 40 hours after the first transfection 5 ml of cell culture media were added to each plate. We analyzed knock down efficiency with western blot (anti-METTL3 Polyclonal antibody, protein tech Catalog.number: 15073-1-AP) and continued with BrU-Chase Seq 72 hours after the first hit. The experiment was performed in duplicates.

Transcript m6A-level and splicing index

The m6A level per transcript from the qTNTchase-seq experiment were calculated as described in (Molinie et al., 2016). The ratio of the RNA abundance for each transcript between the eluate and the supernatant was represented by the ratio of the overlapping strand-specific RNA read counts normalized to the ratio of the reads of the ERCC RNAs. We used the log2-transformed read counts of ERCC RNAs to fit a linear regression model, computing the eluate ERCC reads as a function of the supernatant ERCC reads with a coefficient of 1 (not shown). The log2 ratio between ERCC eluate counts and supernatant counts was

indicated by the intercept of the regression formula. Only the ERCC RNAs with at least 100 read counts were used in this pipeline.

M6A level = E/(E+S*2^*intercept*)

Eluate read counts (*E*), supernatant read counts (*S*), and the intercept of ERCC regression (*intercept*)

We assessed the splicing efficiency per transcript as the ratio of the overlapping strand-specific split reads (extracted by using bedtools coverage –s –F 1.0) to all (split + non-split) reads covering the transcript.

Quantitative real-time PCR

RNA was reverse transcribed using the GoScript reverse transcription Promega A500. cDNA was quantified on an 7900HT Fast real time PCR system (Applied Biosystems) using the Go Taq qPCR Master Mix Promega (A6001). The PCR was carried out using a standard protocol with melting curve. Primers for unspliced RNA transcripts were design to span exon – intron 5' splice junction and exon – exon boundaries for spliced RNA transcripts. Splicing efficiency (SE) was determined by the ration of $2^{-CT_{spliced}}$ / ($2^{-CT_{spliced}}+2^{-CT_{unspliced}}$) for each timepoint. SED was determined by the ration of SED = 1/ ((1- SE0 min) * (1- SE60 min))

RNA sequencing and data analysis

For the BrU-Chase Seq, the library preparation was performed using the TrueSeq Stranded Total RNA Kit (Illumina). Sequencing was performed on an Illumina HiSeq 2500 instrument to obtain around 200M reads per sample. For the TNT-Seq, 100 ng of Input BrU-labeled fragmented RNA and 100 ng of TNT-IP eluate RNA were subjected to library preparation following the TruSeq Stranded mRNA Library Preparation Kit instructions with some modifications. The protocol started from the first strand synthesis step and 3X Clean-NA-Beads beads volume was used for the buffer exchange to include shorter RNA fragments.

Mapping of strand-specific reads to GRC37 genome assembly (hg19) was done using STAR (Dobin et al., 2013) and only uniquely mapped reads were kept for further downstream analyses. To extract read coverage per nucleotide position across the genome the strand-specific bed files were sorted by chromosome and start coordinate and converted into wig files with bedtools genomecov using –scale to normalize for library size. To assess the genome-wide correlation of the m6A signal from replicates, the ratio of normalized read counts per nucleotide position of IP to Eluate, rendering the m6A signal, was converted to bigWig using wigToBigWig (UCSC) and then bigWigCorrelate (UCSC) was used. To extract the m6A signal per nucleotide position in given intervals, the depth at each nucleotide position of the examined intervals (e.g. within +/- 500 bp windows around anchor points) was extracted using bedtools coverage –d –s from the m6A Input and the respective m6A IP, and then the ratio m6A IP/Input multiplied by (total number of mapped reads in the Input/ total number of mapped reads in the IP) was calculated. Then the average m6A signal was extracted at each nucleotide position from all examined entries.

m6A peak calling

We called m6A peaks based on a previously published pipeline (Ke et al., 2015; Ke et al., 2017). We first divided the genome into 20 bp non-overlapping bins with bedtools windowMaker and extracted the strand-specific read coverage from m6A Input and IP for all bins using bedtools coverageBed –s. Fisher's exact test p-value was extracted from the matrix (bin Input read counts, bin IP read counts, total number of mapped reads in the Input, total number of mapped reads in the IP) and adjusted by the Benjamini and Hochberg method to determine the false discovery rate (FDR). Only windows with a p-adjusted < 0.05 in all three replicates and fold enrichment (score) minimum four in at least two out of the three replicates were kept as significant. Adjacent significant bins were merged using bedtools mergeBed into broader peaks (finally 95 % of the peaks were in the range 20-100 nt long). In the case of

broad peaks, the peak summit is the midpoint of the 20 nt window with the maximum score, or the midpoint of the interval of merged adjacent bins sharing same maximum score within the same peak. In a few cases, a broad peak was assigned more than one summits if it contained non-adjacent windows sharing the same maximum score, finally yielding 58102 m6A peaks and 58311 peak summits. Custom scripts were written in awk programming language.

De novo motif search

De novo motif search was run using HOMER (Heinz et al., 2010) within +/-150 nt intervals around the peak summit of 5651 best scoring exonic m6A peaks (minimum fold enrichment 20) and the same number of top best intronic peaks. Control sequences were generated from the respective input sequences with the scrambleFasta.pl script. Then, *de novo* motif search was run with 'findsMotifs.pl input_sequences.fa fasta –basic –rna –len 6,7,8 –fasta scrambled_sequences'. The results were inspected in terms of enrichment, significance and the presence of common consensus sequences, with the four motifs displayed in Figure 1B being the most represented. Those were used to scan the input sequences for the presence of match occurrences using the 'dna-pattern' search tool from the RSAT suite (Medina-Rivera et al., 2015) with parameters 'search given strand only, prevent overlapping matches, origin-start, return flanking nucleotide positions 2'. Motif search was also performed in the same number of random genomic intervals as a control, generated with bedtools (–length 300 –number 5651). The matches were aligned and the logo was generated with WebLogo3 (Crooks et al., 2004) .

Splicing kinetics and predictive models

To assess splicing efficiency we extracted the splicing index value θ as in (Mukherjee et al., 2017). θ equals to the ratio of the split reads mapping to the 5' and 3' SJ of an intron divided

to the sum of split plus non-split reads (schematic representation in Figure 2A). The θ value (representing Splicing Efficiency, SE) was extracted from all pulse-chase time points, for 13,532 introns with at least five reads coverage at both 5' and 3' SJ, and used in k-means clustering with k = 3 to call three groups of distinct splicing efficiency (fast, medium and slow) (Supplementary Figure 2B). The Splicing Efficiency Dynamics metric was calculated as SED = 1/ ((1.001- θ 0 min) * (1.001- θ 60 min)) (plotted in the *log* scale for the three groups in Figure 2F). To assess constitutive versus alternative splicing we extracted the ψ value as in (Mukherjee et al., 2017). ψ is the ratio of constitutive split reads assigned to a given intron's 5' and 3' SJ to all split reads (i.e. split reads from the given intron 5' SJ to any downstream 3'SJ and from the intron's 3' SJ to any upstream 5' SJ, as depicted in Figure 2A). Therefore ψ is in the range 0 to 1 with 1 meaning 100 % constitutive splicing. We then used the ψ value extracted from the pulse-chase time point 60 min (closer to steady-state) to perform k-means clustering with k = 2 and define two clusters of introns, constitutive (n = 11836, minimum ψ 0.5294) and alternative (n = 1696, maximum ψ 0.5278). In the case of introns classified as alternative spliced (ψ < 0.5278) upstream or downstream exon skipping takes place.

The following features were used in logistic and linear regression models to predict splicing efficiency kinetics and alternative versus constitutive splicing:

The 5' and 3' splice site underlying sequence scores extracted using MaxEntScan (http://genes.mit.edu/burgelab/maxent/Xmaxentscan_scoreseq.html); distance of the 5' SJ to the annotated transcript first start site (TSS) and of the 3' SJ to the last end site (TES); expression calculated as coverage (reads per kb) from the m6A Input RNA-seq (15 min BrU pulse) for the whole transcript interval where the intron belongs to; intron length; intron overall m6A signal extracted as the strand-specific m6A IP read coverage divided to m6A Input read coverage, normalized by (total number of mapped m6A Input reads * total number

of mapped m6A IP reads); m6A signal calculated the same way at the 5' SJ 100 nt exonic boundary, 5' SJ 100 nt intronic boundary, 3' SJ 100 nt exonic boundary and 3' SJ 100 nt intronic boundary.

To predict fast versus slow or alternative versus constitutive splicing, logistic regression was performed with R function glm (family = binomial) (all parameters apart from the sequence scores were first log scale transformed and all were then standardized). To evaluate the fitting of the model and assess discrimination, the Receiver Operating Characteristic Curve (ROC) and the area under the curve (AUC) were calculated with the R package ROCR (Sing et al., 2005). Linear regression to predict splicing efficiency using the continuous value θ (in the range 0 to 1) was performed with R function lm().

CLIP data analysis

We used CLIP data for SRF3 and SRSF10 from (Xiao et al., 2016)(GEO GSE71096). To calculate the relative SRSF10/SRSF3 binding per nucleotide position, we used the ModeScore column from the GEO submitted PARalyzer output file, which is the score of the highest signal divided to the sum value (signal+backround) and ranges from 0.5 to 1. We first extracted the coverage for each SRSF per nucleotide position in the +/-500 nt window around 5' or 3' SJ, or per bin for the length-binned introns (introns with length 1000-10,000 nt, binned into 1000 non-overlapping windows), by using bedtools coverage –s –d. Nucleotide positions with overlapping CLIP binding sites were assigned the cluster's score (ModeScore column) whereas nucleotide positions with no CLIP data overlap were assigned a pseudo-score 0.1. We then computed the ratio SRFS10/SRSF3 per nucleotide position or per bin of all analyzed loci and the metagene analysis extracting the average ratio SRFS10/SRSF3 per nucleotide position or per bin was run separately for each of the subgroups fast/medium/slow or constitutive/alternative.

Table 1: Primer Sequences. All the primers and siRNAs where purchased from Integrated DNA Technology, Inc. (IDT)

RT-PCR and qPCR primers

NAME	**Sequence**
CDKN1B unspliced Forward	AATAAGGAAGCGACCTGCAA
CDKN1B unspliced Reverse	atacgccgaaaagcaagcta
CDKN1B spliced Forward	AATAAGGAAGCGACCTGCAA
CDKN1B spliced Reverse	GGGGAACCGTCTGAAACAT
LMAN2 unspliced Forward	GTGACTGCGGATATAACTGACG
LMAN2 unspliced Reverse	ctcgccctcactcttcactc
LMAN2 spliced Forward	GTGACTGCGGATATAACTGACG
LMAN2 spliced Reverse	ATAGTGCTGCCCTGGAAGTC
NASP unspliced Forward	CATGGAGTCCACAGCCACT
NASP unspliced Reverse	tgccttaagctttccacagtc
NASP spliced Forward	CATGGAGTCCACAGCCACT
NASP spliced Reverse	GCAGATGTAGAAGGAGCAGGA
ARF4 unspliced Forward	CCTCCCTCTTCTCCCGACT
ARF4 unspliced Reverse	attgtggagaccctgccttt
ARF4 spliced Forward	CCTCCCTCTTCTCCCGACT
ARF4 spliced Reverse	TTGTCTTGCCAGCAGCATC
C8orf33 Forward	TAAGAAGAAAACGCGGAACAGG
C8orf33 Reverse	GGTGGGTTTCTGCCTCTTGA
MSN unspliced Forward	TCAAGAAGCTGAAGAGGCCA
MSN unspliced Reverse	agttcccataatcccagccc
MSN spliced Reverse	CTGTCAGCTCTGCCATTTCC

SPTBN1 unspliced Forward	CTGGATGAGCGAGCAGGAG
SPTBN1 unspliced Reverse	aagtgtgcccagggtttgaa
SPTBN1 spliced Revers	GCATAGTCCTCCACAGCTTGT
NOL7 unspliced Forward	TCCTGAAGGAGAAGAGGAAGC
NOL7 unspliced Forward	aattctccctgagccgagtt
NOL7 spliced Forward	AACGCTCCTGAAGGAGAAGA
NOL7 spliced Reverse	TCCAAAATAGTGTCTGGAAGGA

NAME siRNA Target	**Sequence 5'→3'**
Mettl3-1	5'-ACUGCUCUUUCCUUAAUA 5'-AAACAUGUAUUAAGGAAA
Mettl3-2	5'-CCAACAGUCCACUAAGGA 5'-CUGUUGUUCCUUAGUGGA
Mettl3-3	5'-AGGCAAGGAACAAUCCAU 5'-UUCAACAAUGGAUUGUUC
Mettl3-4	5'-AGCCAAGGAACAAUCCAU 5'-UUCAACAAUGGAUUGUUC
Control	NCI IDT controls

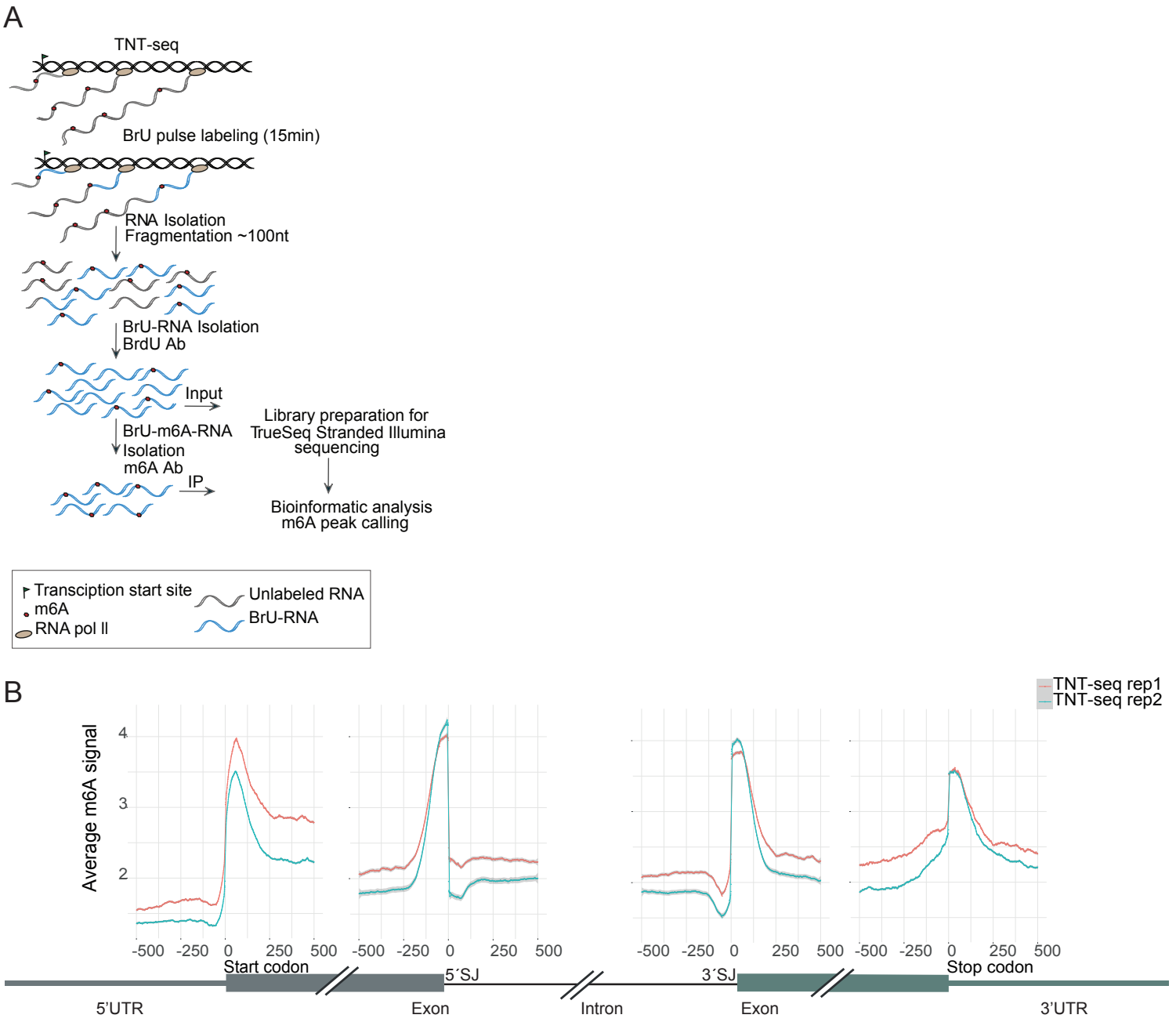

Figure S1;Related to Figure 1:m6A signal and motif analysis
(A) Schematic representation of the TNT-seq protocol. (B) The average m6A signal per nucleotide position around start and stop codons, 5' and 3' SJs is shown. (C-D) m6A peak distribution in (C) newly transcribed RNA and (D) mRNA(Schwartz et al., 2014)

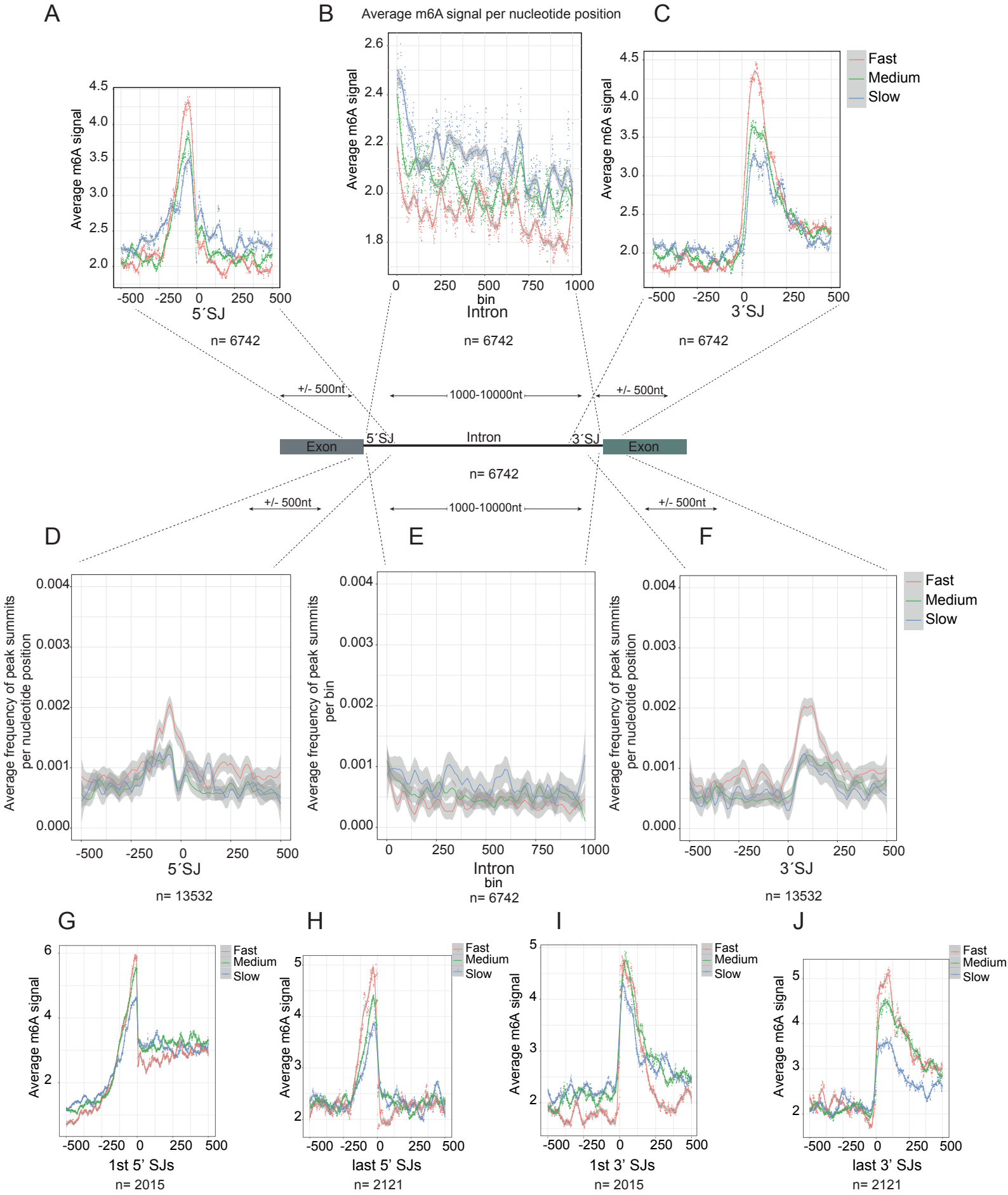

Figure S2; Related to Figure 2: M6A signal and splicing kinetics (A-C) Average m6A signal per nucleotide position in the window +/-500 nt around (A) 5´SJ and (C) 3´SJ and (B) internally per bin for 6742 introns (with length 1000-10000 nt), for fast, medium and slow processed introns. (D-F) Average frequency of m6A peak summits per nucleotide position in the window +/- 500 nt around (D) 5' SJ, (F) 3' SJ of all 13,532 filtered introns, and (E) per bin of 6722 introns 1000-10000 nt long, extracted separately for fast, medium, slow subgroups. The lines represent loess curve fitting (local polynomial regression) with the 95% confidence interval grey shaded.(G-J) Average m6A signal per nucleotide position around the 5' and 3' SJs of only the first and last introns.n = number of introns

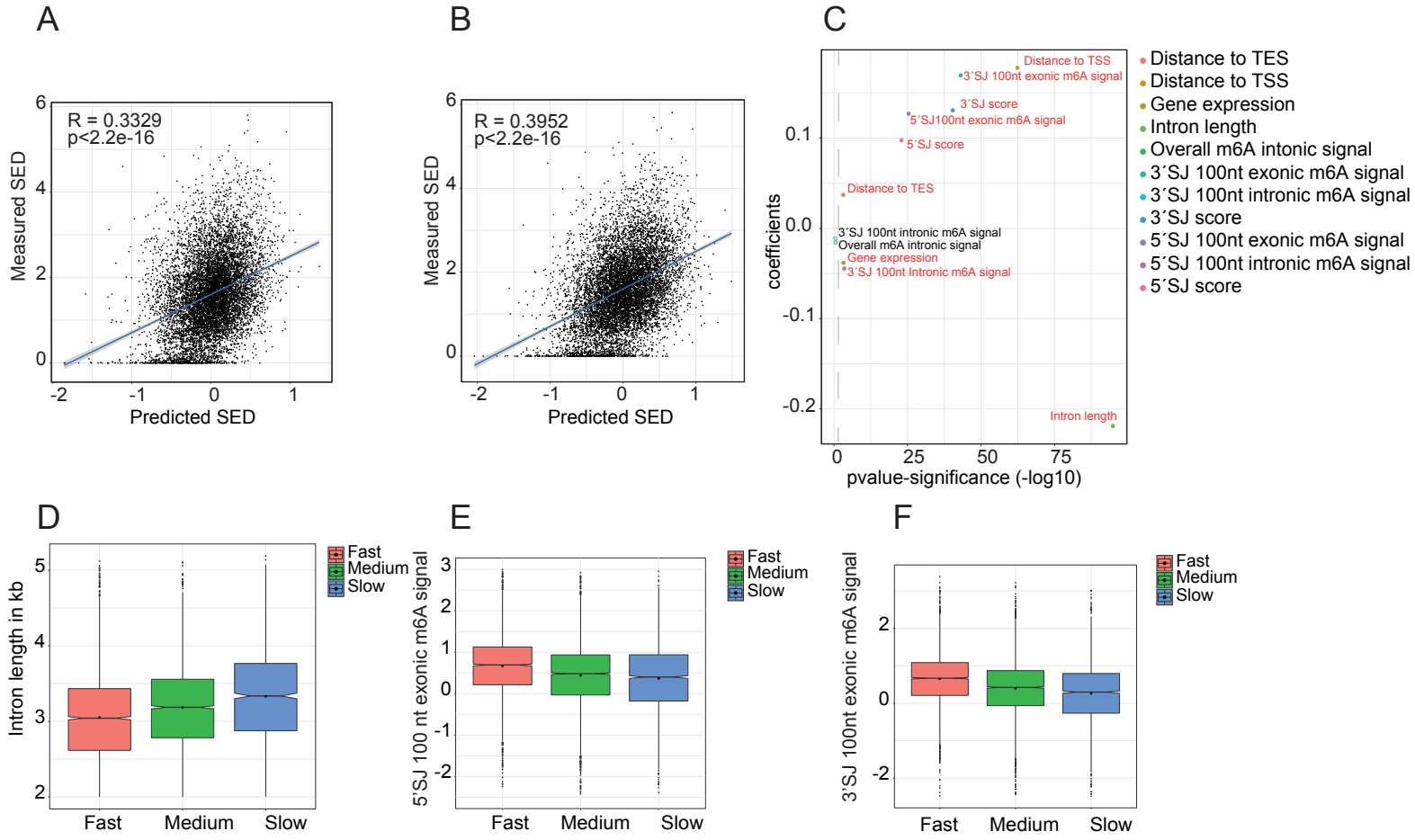

Figure S3; Related to Figure 2:Prediction of SED in a linear regression model
(A-C) Prediction of Splicing Efficiency Dynamics (SED) (as a continuous value) from (A) all features excluding m6A data (B) including m6A data using linear regression. The line indicates the linear regression fit between predicted and measured SED and the correlation value (R) with the associated significance is indicated.
(C) Plot depicting the contribution of each feature to the linear fit predicting SED. (D) Boxplots depicting the distribution of intron length for the three groups Fast (pink), Medium (Green) and Slow (blue) introns.
(E) Boxplots depicting the distribution of the m6A signal in the 100 nt exonic window boundary adjacent to the 5'SJ, for the three groups. (F) Boxplots depicting the distribution of the m6A signal in the 100 nt exonic window boundary adjacent to the 3'SJ, for the three groups.

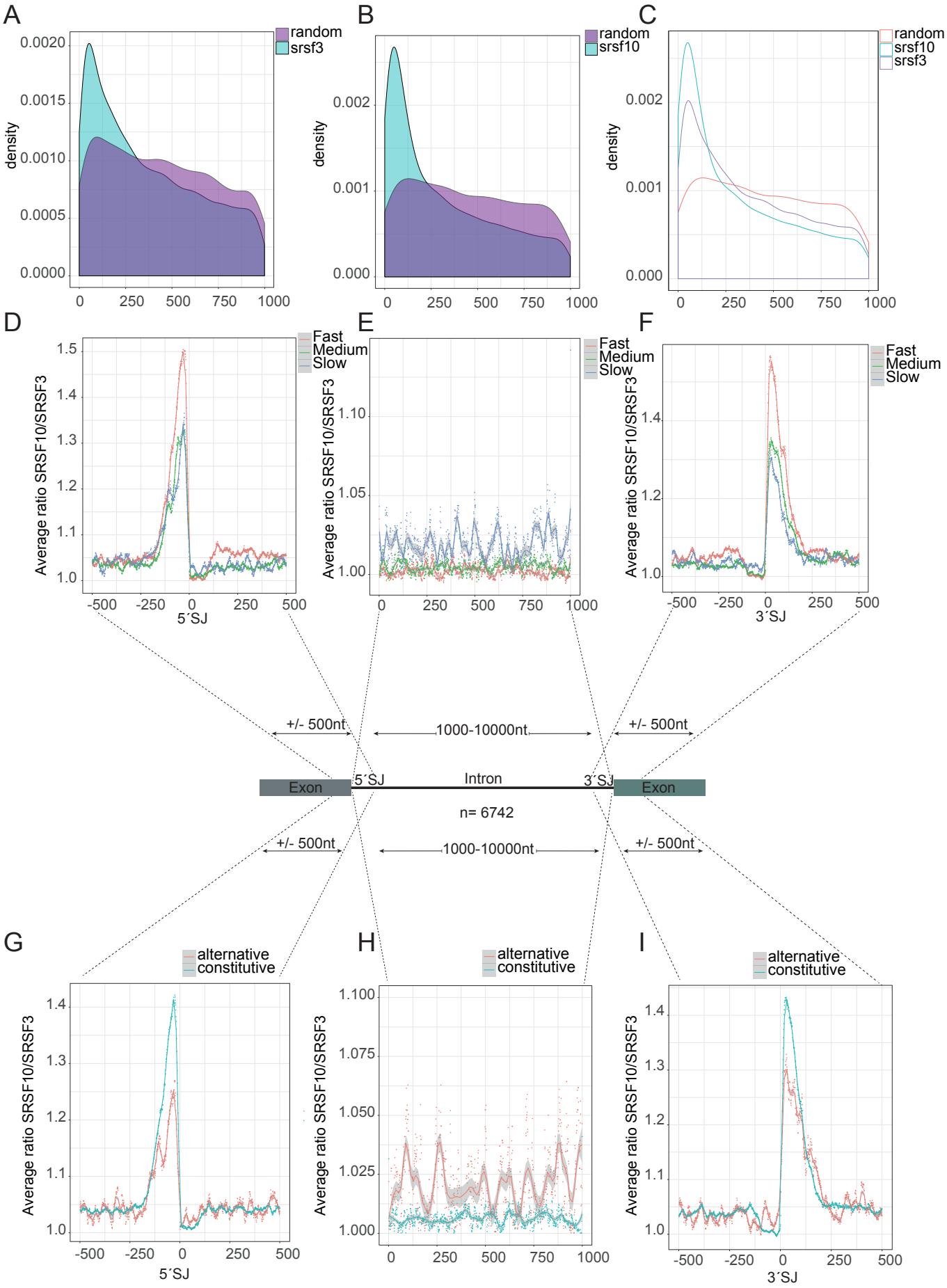

Figure S4; Related to Figure 2 and 3: Splicing factors coincide with m6A deposition
(A-C) Distribution of the interdistances of factor binding sites to closest m6A peak summit for (A) SRSF3 (B) SRSF10 and (C) overlap. As a control, distance from the midpoint of the respectively same number of randomly generated genomic intervals is also plotted. (D-F) Distribution of the average ratio SRSF10/SRSF3 binding, extracted separately for the three subgroups fast/medium/slow per nucleotide position in the window +/-500 nt around the 5'SJ (D) and 3'SJ (F), or per bin (E) for 6,742 length-binned introns (with a length 1,000-10,000 nt). (G-I) Same analysis as in (D-F) but comparing the average SRSF10/SRSF3 ratio for the two subgroups constitutive versus alternative.

References

Crooks, G.E., Hon, G., Chandonia, J.-M., and Brenner, S.E. (2004). WebLogo: A Sequence Logo Generator. Genome Research *14*, 1188-1190.

Dobin, A., Davis, C.A., Schlesinger, F., Drenkow, J., Zaleski, C., Jha, S., Batut, P., Chaisson, M., and Gingeras, T.R. (2013). STAR: ultrafast universal RNA-seq aligner. Bioinformatics *29*, 15-21.

Heinz, S., Benner, C., Spann, N., Bertolino, E., Lin, Y.C., Laslo, P., Cheng, J.X., Murre, C., Singh, H., and Glass, C.K. (2010). Simple Combinations of Lineage-Determining Transcription Factors Prime cis-Regulatory Elements Required for Macrophage and B Cell Identities. Molecular Cell *38*, 576-589.

Ke, S., Alemu, E.A., Mertens, C., Gantman, E.C., Fak, J.J., Mele, A., Haripal, B., Zucker-Scharff, I., Moore, M.J., Park, C.Y.*, et al.* (2015). A majority of m6A residues are in the last exons, allowing the potential for 3' UTR regulation. Genes Dev *29*, 2037-2053.

Ke, S., Pandya-Jones, A., Saito, Y., Fak, J.J., Vågbø, C.B., Geula, S., Hanna, J.H., Black, D.L., Darnell, J.E., and Darnell, R.B. (2017). m6A mRNA modifications are deposited in nascent pre-mRNA and are not required for splicing but do specify cytoplasmic turnover. Genes & Development *31*, 990-1006.

Medina-Rivera, A., Defrance, M., Sand, O., Herrmann, C., Castro-Mondragon, J.A., Delerce, J., Jaeger, S., Blanchet, C., Vincens, P., Caron, C.*, et al.* (2015). RSAT 2015: Regulatory Sequence Analysis Tools. Nucleic Acids Research *43*, W50-W56.

Molinie, B., Wang, J., Lim, K.S., Hillebrand, R., Lu, Z.-x., Van Wittenberghe, N., Howard, B.D., Daneshvar, K., Mullen, A.C., Dedon, P.*, et al.* (2016). m6A-LAIC-seq reveals the census and complexity of the m6A epitranscriptome. Nat Meth *13*, 692-698.

Mukherjee, N., Calviello, L., Hirsekorn, A., de Pretis, S., Pelizzola, M., and Ohler, U. (2017). Integrative classification of human coding and noncoding genes through RNA metabolism profiles. Nat Struct Mol Biol *24*, 86-96.

Paulsen, M.T., Veloso, A., Prasad, J., Bedi, K., Ljungman, E.A., Tsan, Y.C., Chang, C.W., Tarrier, B., Washburn, J.G., Lyons, R.*, et al.* (2013). Coordinated regulation of synthesis and stability of RNA during the acute TNF-induced proinflammatory response. P Natl Acad Sci USA *110*, 2240-2245.

Sing, T., Sander, O., Beerenwinkel, N., and Lengauer, T. (2005). ROCR: visualizing classifier performance in R. Bioinformatics *21*, 3940-3941.

Xiao, W., Adhikari, S., Dahal, U., Chen, Y.-S., Hao, Y.-J., Sun, B.-F., Sun, H.-Y., Li, A., Ping, X.-L., Lai, W.-Y.*, et al.* (2016). Nuclear m6A Reader YTHDC1 Regulates mRNA Splicing. Molecular Cell *61*, 507-519.